



A simple and explicit numerical method for the phase-field model for diblock copolymer melts

Junxiang Yang^a, Chaeyoung Lee^b, Darae Jeong^c, Junseok Kim^{b,*}

^a School of Computer Science and Engineering, Sun Yat-sen University, Guangzhou 510275, China

^b Department of Mathematics, Korea University, Seoul, 02841, Republic of Korea

^c Department of Mathematics, Kangwon National University, Gangwon-do 24341, Republic of Korea

ARTICLE INFO

Keywords:

Explicit finite difference method
Diblock copolymer melts
Saul'yev-type method

ABSTRACT

In this paper, we present a simple and explicit finite difference method for the phase-field model for diblock copolymer melts. A diblock copolymer is a polymer consisting of two types of different monomers bonded covalently to each other to form a single copolymer chain. When the temperature is below the critical temperature, the copolymer melt exhibits microphase separation. The mathematical model is derived from a total free energy functional which contains kinetic, gradient, double well, and long-range nonlocal potentials. The Saul'yev-type scheme based on a linearly stabilized convex splitting method is used for the discretizations. The proposed method is simple and computationally efficient because the scheme is explicit and it does not require any iterative procedures. The proposed scheme not only overcomes the severe time step restriction for the explicit scheme but also works well for the simulations of lamellar and hex-cylinder structures which are characteristic morphologies for diblock copolymer melts after phase separation. Furthermore, the proposed method can be easily applied to the simulations in complex computational domains. We present various numerical tests to demonstrate the performance of the proposed scheme.

1. Introduction

In this article, we present a simple and computationally efficient explicit finite difference method (FDM) for the nonlocal Cahn–Hilliard (CH) equation for diblock copolymer melts [1,2]:

$$\frac{\partial \phi(\mathbf{x}, t)}{\partial t} = \Delta [F'(\phi(\mathbf{x}, t)) - \epsilon^2 \Delta \phi(\mathbf{x}, t)] - \alpha(\phi(\mathbf{x}, t) - \bar{\phi}), \quad \mathbf{x} \in \Omega, \quad t > 0. \quad (1)$$

In a domain $\Omega \subset \mathbb{R}^2$, $\phi(\mathbf{x}, t)$ is the difference of the local volume fraction of *A* and *B* monomers. Here, $F(\phi) = 0.25(\phi^2 - 1)^2$ is the double-well free energy that has two minima at $\phi = \pm 1$, ϵ is the gradient energy coefficient, α is the positive parameter, and $\bar{\phi} = \int_{\Omega} \phi(\mathbf{x}, 0) d\mathbf{x} / \int_{\Omega} d\mathbf{x}$. Eq. (1) can be derived from the H^{-1} gradient flow for the following total energy functional:

$$\mathcal{E}(\phi) = \int_{\Omega} \left(F(\phi) + \frac{\epsilon^2}{2} |\nabla \phi|^2 \right) d\mathbf{x} + \frac{\alpha}{2} \int_{\Omega} \int_{\Omega} G(\mathbf{x} - \mathbf{y})(\phi(\mathbf{x}) - \bar{\phi})(\phi(\mathbf{y}) - \bar{\phi}) d\mathbf{y} d\mathbf{x}. \quad (2)$$

Here, $G(\mathbf{x})$ is given by the solution of the Poisson problem $-\Delta G(\mathbf{x}) = \delta(\mathbf{x})$ with a Dirac delta function $\delta(\mathbf{x})$. We note that the L^2 -gradient flow approach for energy functional (2) generates the Allen–Cahn type

dynamics. The Allen–Cahn type diblock copolymer model has weaker CFL condition and is relatively easier to solve numerically than the CH type model. Various studies for the Allen–Cahn type model can be found in Refs. [3–6].

Returning to the CH type model (1), there have been many studies for the numerical approach. In Refs. [7–9], the authors proposed a novel stabilized scalar auxiliary variable (SAV) approach which is second-order accurate, provably unconditionally energy stable, non-iterative for the CH type diblock copolymer model. In Ref. [10], the authors presented an unconditionally energy stable and second-order accurate numerical method by combining a Crank–Nicolson type scheme with a nonlinearly stabilized splitting scheme. Tenneti et al. [11] studied equilibrium microstructures exhibited by diblock copolymers in confined three-dimensional geometries using a finite element method.

Jeong et al. [12] proposed a numerical method for finding energy-minimizing wavelengths of equilibrium states for diblock copolymers. Jeong and Kim [13] presented a computational scheme for microphase separation pattern formations in diblock copolymers on curved surfaces. Recently, Li et al. [14] developed an efficient method for restoring damaged fingerprint image using the non-local CH equation. For the

* Corresponding author.

E-mail address: cfdkim@korea.ac.kr (J. Kim).

URL: <https://mathematicians.korea.ac.kr/cfdkim> (J. Kim).

numerical solvers of the non-local CH equation, there have been developed various methods such as Fourier-spectral method [15], multigrid method [16]. Because the non-local CH equation is very similar to the local CH equation, we can use most of numerical solvers for the local CH equation.

The primary purpose of this study is to present a simple and explicit FDM for the phase-field model for diblock copolymer melts. The mathematical model is a four-order partial differential equation. Therefore, if we use a fully explicit Euler's method, then the time step restriction is very stringent. To overcome this severe time step restriction, we apply the Saul'yev-type scheme based on a linearly stabilized convex splitting method. In addition, the proposed method can be easily applied to the simulations in complex computational domains because it is explicit.

The contents of this paper are as follows. We describe the proposed numerical method in Section 2. Several computational experiments are given to show the capability of the proposed method in Section 3. In Section 4, we discuss the extension of the proposed method to a possible second-order time-accurate scheme. In Section 5, we conclude.

2. Discretization

Let $\Omega = (a, b) \times (c, d)$ be the domain and $\Omega_h = \{(x_i = a + (i-0.5)h, y_j = c + (j-0.5)h) \mid i = 1, \dots, N_x, j = 1, \dots, N_y\}$ be the discrete numerical domain, where h is the space step size; N_x and N_y are integers. Let ϕ_{ij}^n be the numerical solution of $\phi(x_i, y_j, n\Delta t)$, where Δt is the time step. Let us consider the linear convex splitting-type scheme [17]:

$$\frac{\phi_{ij}^{n+1} - \phi_{ij}^n}{\Delta t} = \Delta_d[(\phi_{ij}^n)^3 - 3\phi_{ij}^n] + 2\Delta_d\phi_{ij}^{n+1} - \epsilon^2\Delta_d^2\phi_{ij}^{n+1} - \alpha(\phi_{ij}^{n+1} - \bar{\phi}), \quad (3)$$

where $\Delta_d\phi_{ij} = (\phi_{i-1,j} + \phi_{i+1,j} - 4\phi_{ij} + \phi_{i,j-1} + \phi_{i,j+1})/h^2$ and $\Delta_d^2\phi_{ij}$ is defined similarly. Unless otherwise specified, the following discrete homogeneous Neumann boundary condition is used:

$$\begin{aligned} \phi_{-1,j}^n &= \phi_{2j}^n, \quad \phi_{0j}^n = \phi_{1j}^n, \quad \phi_{N_x+1,j}^n \\ &= \phi_{N_x,j}^n, \quad \phi_{N_x+2,j}^n = \phi_{N_x-1,j}^n, \quad \text{for } j = 1, \dots, N_y, \\ \phi_{i,-1}^n &= \phi_{i,2}^n, \quad \phi_{i,0}^n = \phi_{i,1}^n, \quad \phi_{i,N_y+1}^n \\ &= \phi_{i,N_y}^n, \quad \phi_{i,N_y+2}^n = \phi_{i,N_y-1}^n, \quad \text{for } i = 1, \dots, N_x. \end{aligned}$$

Then, we apply the following Saul'yev-type scheme [18,19] for Eq. (3):

$$\text{For } j = 1, 2, \dots, N_y, \quad \text{for } i = 1, 2, \dots, N_x, \quad (4)$$

$$\begin{aligned} \frac{\phi_{ij}^{n+1} - \phi_{ij}^n}{\Delta t} &= \Delta_d[(\phi_{ij}^n)^3 - 3\phi_{ij}^n] + \frac{2}{h^2} (\phi_{i-1,j}^{n+1} + \phi_{i+1,j}^n - 2\phi_{ij}^n - 2\phi_{ij}^{n+1} \\ &\quad + \phi_{i,j-1}^{n+1} + \phi_{i,j+1}^n) - \frac{\epsilon^2}{h^4} [\phi_{i-2,j}^{n+1} + \phi_{i+2,j}^n + \phi_{i,j-2}^{n+1} + \phi_{i,j+2}^n \\ &\quad + 2(\phi_{i-1,j-1}^{n+1} + \phi_{i-1,j+1}^n + \phi_{i+1,j-1}^{n+1} + \phi_{i+1,j+1}^n) \\ &\quad - 8(\phi_{i-1,j}^{n+1} + \phi_{i+1,j}^n + \phi_{i,j-1}^{n+1} + \phi_{i,j+1}^n) + 10\phi_{ij}^n + 10\phi_{ij}^{n+1}] \\ &\quad - \alpha(\phi_{ij}^{n+1} - \bar{\phi}). \end{aligned} \quad (5)$$

We can simplify Eq. (5) as

$$\begin{aligned} \phi_{ij}^{n+1} &= \frac{1}{r} \left\{ \frac{\phi_{ij}^n}{\Delta t} + \Delta_d[(\phi_{ij}^n)^3 - 3\phi_{ij}^n] + \frac{2}{h^2} (\phi_{i-1,j}^{n+1} + \phi_{i+1,j}^n - 2\phi_{ij}^n \right. \\ &\quad \left. + \phi_{i,j-1}^{n+1} + \phi_{i,j+1}^n) - \frac{\epsilon^2}{h^4} [\phi_{i-2,j}^{n+1} + \phi_{i+2,j}^n + \phi_{i,j-2}^{n+1} + \phi_{i,j+2}^n \right. \\ &\quad \left. + 2(\phi_{i-1,j-1}^{n+1} + \phi_{i-1,j+1}^n + \phi_{i+1,j-1}^{n+1} + \phi_{i+1,j+1}^n) \right. \\ &\quad \left. - 8(\phi_{i-1,j}^{n+1} + \phi_{i+1,j}^n + \phi_{i,j-1}^{n+1} + \phi_{i,j+1}^n) + 10\phi_{ij}^n \right\} + \alpha\bar{\phi}, \end{aligned} \quad (6)$$

where $r = 1/\Delta t + 4/h^2 + 10\epsilon^2/h^4 + \alpha$. There are the other 7 cases for loops:

$$\text{For } j = 1, 2, \dots, N_y, \quad \text{for } i = N_x, N_x - 1, \dots, 1, \quad (7)$$

$$\text{For } j = N_y, N_y - 1, \dots, 1, \quad \text{for } i = 1, 2, \dots, N_x, \quad (8)$$

$$\text{For } j = N_y, N_y - 1, \dots, 1, \quad \text{for } i = N_x, N_x - 1, \dots, 1, \quad (9)$$

Table 1

Possible maximum time steps ensuring stable computation.

Space step h :	1/16	1/32	1/64	1/128
present scheme:	2.10e-3	2.00e-3	2.00e-3	2.10e-3
fully explicit scheme:	2.29e-6	1.91e-6	1.79e-6	3.72e-7

Table 2

CPU times for the fully explicit and proposed schemes.

Space step h :	1/75	1/150	1/225
CPU^e :	59.158	245.730	687.495
Ratio:	84.151	95.615	100.570
CPU :	0.703	2.570	6.836

$$\text{For } i = 1, 2, \dots, N_x, \quad \text{for } j = 1, 2, \dots, N_y, \quad (10)$$

$$\text{For } i = N_x, N_x - 1, \dots, 1, \quad \text{for } j = 1, 2, \dots, N_y, \quad (11)$$

$$\text{For } i = 1, 2, \dots, N_x, \quad \text{for } j = N_y, N_y - 1, \dots, 1, \quad (12)$$

$$\text{For } i = N_x, N_x - 1, \dots, 1, \quad \text{for } j = N_y, N_y - 1, \dots, 1. \quad (13)$$

More details can be found in [19], where an explicit conservative Saul'yev scheme for the local CH equation was described.

The main advantages of the proposed scheme compared with other traditional methods are its simplicity and efficiency in dealing with complex domains. Temporal update of the numerical scheme is similar to one iteration of the Gauss-Seidel type iterative. However, it is difficult to show energy stability of the proposed method. Therefore, we present computational tests to demonstrate the energy decrease with practically large time steps.

3. Numerical experiments

Now, we validate the performance of the proposed method through several computational tests. Without specific needs, the computational domain is $\Omega = (0, 2) \times (0, 2)$.

3.1. Comparison study with a fully explicit scheme

The fully explicit scheme is the simplest method to numerically solve the parabolic partial differential equations. However, the time step restriction of the fully explicit method for the nonlocal CH equation is of $O(h^4)$, which is not practical in actual applications. We first study the numerical stability condition. The initial condition is specified as $\phi(x, y, 0) = 0.2 \cos(\pi x) \cos(\pi y)$. Here, various space steps $h = 1/16, 1/32, 1/64, 1/128, \epsilon = 2h$, and $\alpha = 1000$ are used. Numerical solutions are computed until $t = 62.5$. We list the possible maximum time steps in Table 1 with respect to space step h . It can be observed that the proposed scheme obviously releases the strict restriction of the time step.

In addition, we perform the CPU time comparison test. The initial condition is given as $\phi(x, y, 0) = 0.15 \text{rand}(x, y)$, where $\text{rand}(x, y)$ is the random number in $[-1, 1]$. For the fully explicit scheme, we use $\epsilon = 0.01, \alpha = 1000$, and $\Delta t = \delta t$, where $\delta t = 50h^4$ and $h = 1/75, 1/150$, and $1/225$. The simulation stops after 32000 time iterations. For our proposed scheme, we set the time step $\Delta t = 100\delta t$. We define the ratio as CPU^e/CPU , where CPU^e and CPU represent the total CPU time required by the fully explicit and proposed schemes, respectively. Table 2 shows that the proposed method almost saves two orders of the computational time.

Next, we compare the pattern formations simulated by the proposed method with those by the fully explicit method. The initial condition remains unchanged. Here, $\epsilon = 0.01, \alpha = 1000$, and $h = 1/75$ are used. For the fully explicit method, we use $\Delta t = \delta t = 50h^4$. For the proposed method, we consider $\Delta t = 10\delta t, 50\delta t$ and $250\delta t$. The snapshots at $t = 0.05$ are shown in Fig. 1, we can find that the morphology structures are similar, although the time step used in the proposed method is 10

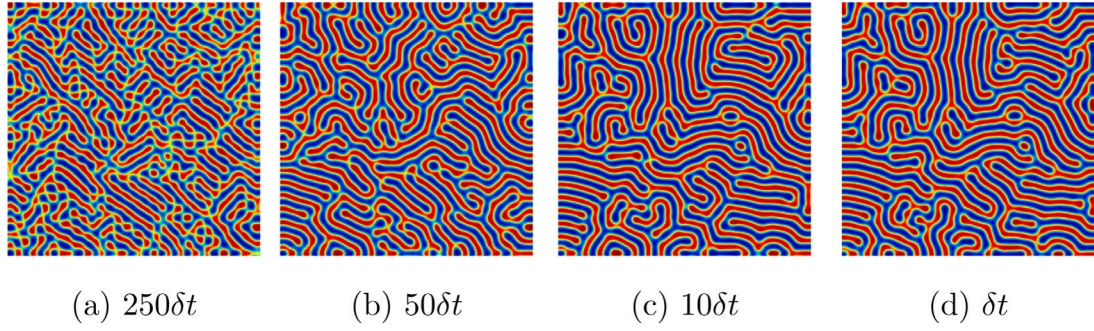


Fig. 1. Snapshots at $t = 0.05$ simulated by our proposed method with various time steps: (a)–(c). The result computed by the fully explicit scheme is shown in (d).

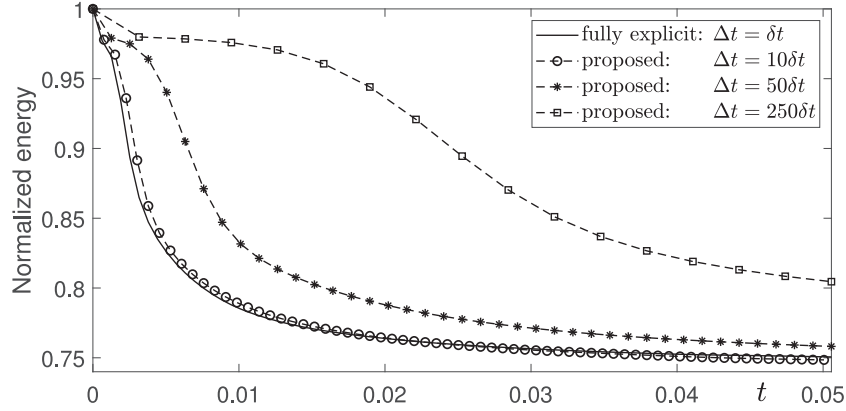


Fig. 2. Normalized energy curves computed by the fully explicit and proposed schemes.

times larger than the time step used in the fully explicit method. Let us define the discrete total energy to be

$$\mathcal{E}(\phi, \psi) = h^2 \sum_{i=1}^{N_x-1} \sum_{j=1}^{N_y-1} \left\{ F(\phi_{ij}) + \frac{\epsilon^2}{2} \left[\frac{(\phi_{i+1,j} - \phi_{ij})^2}{h^2} + \frac{(\phi_{i,j+1} - \phi_{ij})^2}{h^2} \right] + \frac{\alpha}{2} \left[\frac{(\psi_{i+1,j} - \psi_{ij})^2}{h^2} + \frac{(\psi_{i,j+1} - \psi_{ij})^2}{h^2} \right] \right\}, \quad (14)$$

where ψ satisfies $-\Delta\psi = \phi - \bar{\phi}$. The normalized discrete energy is defined as $\mathcal{E}(\phi^n, \psi^n)/\mathcal{E}(\phi^0, \psi^0)$. In Fig. 2, we display the temporal evolutions of the normalized energy curves with respect to various time steps. When $\Delta t = 10\delta t$ is used, the energy curves computed by the proposed and fully explicit methods are similar. Although the energy is non-increasing when we increase the time step, the difference becomes obvious because of the natural discretization error.

3.2. Convergence test

To confirm the temporal and spatial accuracy of the proposed Saul'yev method, we perform the convergence test with respect to time and space. Because the analytical solution is hard to define for the phase-field diblock copolymer model, we compute the successive errors that the numerical solution when Δt and h is compared with that when $\Delta t/4$ and $h/2$. The final time is fixed as $t = n\Delta t = 1.6e - 6$, where n is the iteration number when the time step is Δt . The domain is $\Omega = (0, 1) \times (0, 1)$, the initial state is defined as $\phi(x, y, 0) = 0.5 \tanh\left(\frac{0.3 - \sqrt{(x-0.5)^2 + (y-0.5)^2}}{\sqrt{2}\epsilon}\right)$, and the parameters used are $\epsilon = 0.02$ and $\alpha = 1000$. The discrete error is defined as:

$$e_{ij}^{\Delta t, h} = \psi_{ij}^{\Delta t, h} - \frac{1}{4} \left(\psi_{2i-1, 2j-1}^{\Delta t/4, h/2} + \psi_{2i-1, 2j}^{\Delta t/4, h/2} + \psi_{2i, 2j-1}^{\Delta t/4, h/2} + \psi_{2i, 2j}^{\Delta t/4, h/2} \right),$$

where $\psi_{ij}^{\Delta t, h}$ is the numerical solution ϕ_{ij}^n when the time and space step sizes are used as Δt and h . The convergence rate is defined as

$\log_2(\|e^{\Delta t, h}\|_2 / \|e^{\Delta t/4, h/2}\|_2)$. Here, the discrete L^2 -norm is defined as:

$$\|e\|_2 = \sqrt{\sum_{i=1}^{N_x} \sum_{j=1}^{N_y} e_{ij}^2 / (N_x N_y)}.$$

Table 3 lists the L^2 -errors and the corresponding convergence rates. It can be observed that the proposed method achieves first-order accuracy in time and second-order accuracy in space.

3.3. Effect of average concentration

To investigate the effect of average concentration on the pattern formation, we perform a computational test with the initial condition $\phi(x, y, 0) = \bar{\phi} + 0.15\text{rand}(x, y)$, where $\bar{\phi} = 0$ and $\bar{\phi} = -0.3$ are considered. We use $\Delta t = 0.5h^2$, $h = 1/75$, $\epsilon = 0.01$, and $\alpha = 1000$. In Fig. 3, from top and bottom rows show the snapshots with $\bar{\phi} = 0$ and -0.3 , respectively. We can observe that the lamellar and hex-cylinder structures appear when $\bar{\phi} = 0$ and $\bar{\phi} = -0.3$ are used, respectively. In Fig. 4, the normalized energy curves are plotted. We can find that the energy curves are decreasing in time.

3.4. Effect of α

Now, we study the effect of α value, which is related to the total chain length of the copolymer [20]. Here, the same initial condition and parameters in the previous section are used except $\alpha = 10, 100$, and 1000 . In Fig. 5, the top row shows the snapshots at $t = 12800\Delta t$ with $\bar{\phi} = 0$ and the bottom row shows the results with $\bar{\phi} = -0.3$. As we can observe, the dynamics of the CH model play a dominant role when we decrease the value of α .

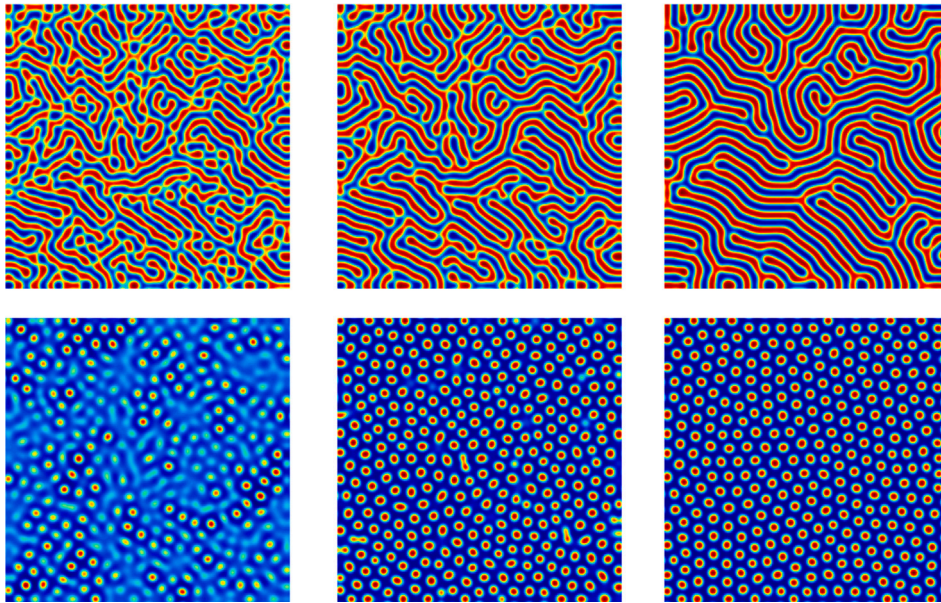


Fig. 3. Top and bottom rows are the results with $\bar{\phi} = 0$ and -0.3 , respectively. From left to right, the snapshots are at $t = 0.0178$, 0.0356 , and 1.1378 .

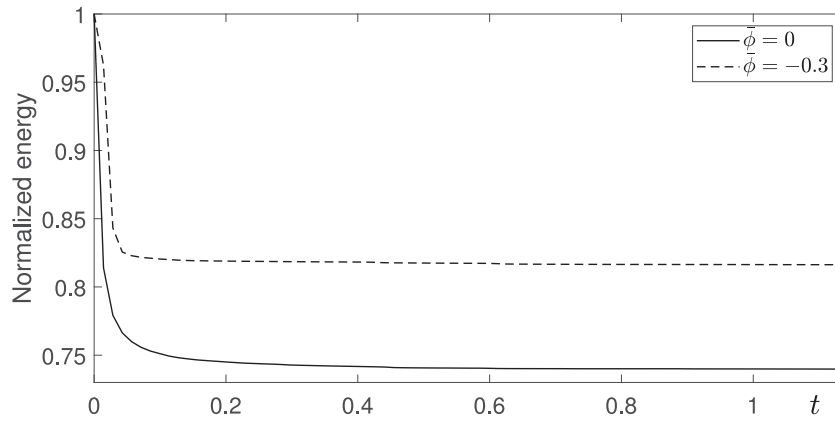


Fig. 4. Normalized energy curves with $\bar{\phi} = 0$ and -0.3 .

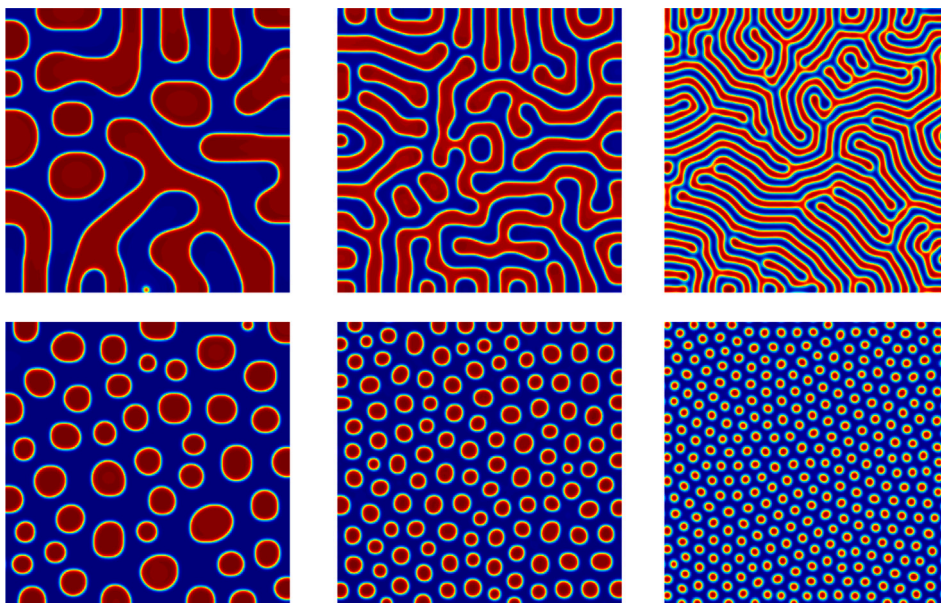


Fig. 5. Snapshots at $t = 12800\Delta t$ with $\bar{\phi} = 0$ (top row) and $\bar{\phi} = -0.3$ (bottom row). From left to right, $\alpha = 10$, 100 , and 1000 , respectively.

Table 3
Discrete L^2 -errors and convergence rates with respect to different time and space steps.

Cases:	(1.000e-6, 1/32) (2.500e-7, 1/64)	Rate	(2.500e-7, 1/64) (6.250e-8, 1/128)	Rate	(6.250e-8, 1/128) (3.125e-8, 1/256)
L^2 -error:	5.505e-3	1.90	1.471e-2	2.01	3.657e-4

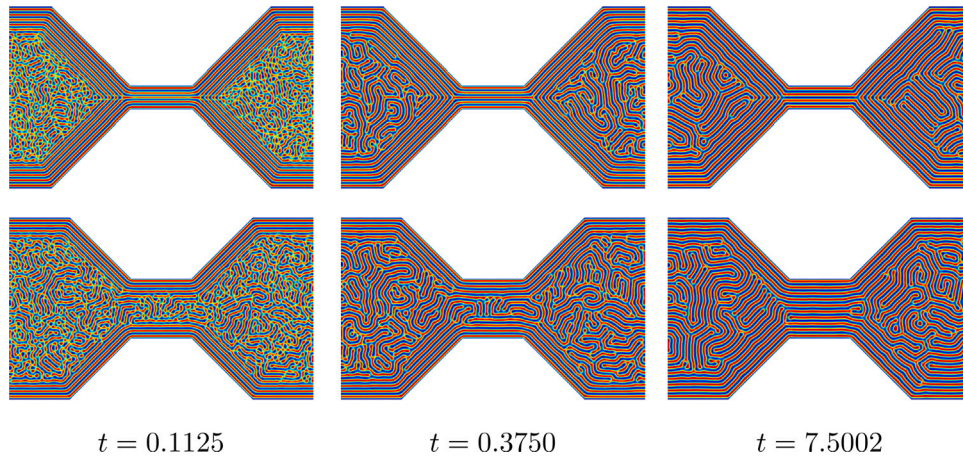


Fig. 6. Effect of channel width. The top and bottom rows are the results with $4L$ and $10L$, respectively.

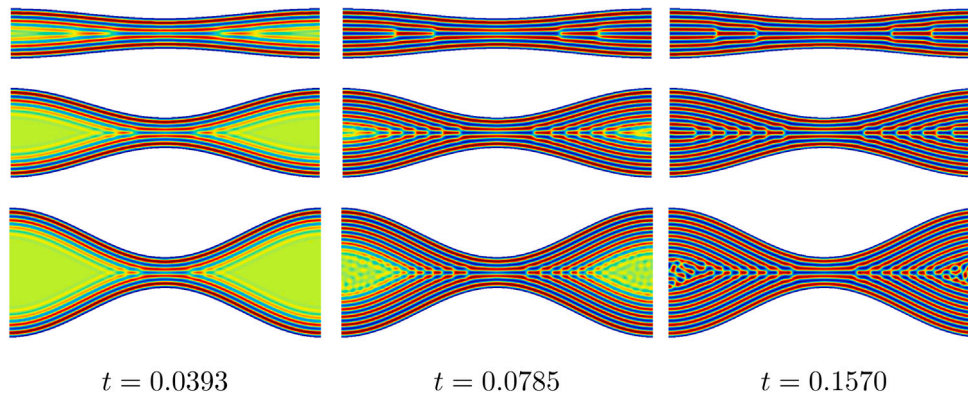


Fig. 7. Pattern formation in the wave-shaped region with respect to different values of A . From top to bottom, $A = 0.2, 0.6,$ and 1 , respectively.

3.5. Local defectiveness control

In this subsection, we consider the local defectiveness control of diblock copolymer patterns [21]. The simulation is performed in a region which is embedded in the full domain $\Omega = (-25L, 25L) \times (-15L, 15L)$, where $L = 0.375$. Here, we use $h = L/10$, $\Delta t = 2.3438e-5$, $\alpha = 100$, and $\epsilon = 1/(20\sqrt{2})$. The Dirichlet boundary value -0.7475 is used. In Fig. 6, the top and bottom rows show the morphology evolutions in the domains with channel width $4L$ and $10L$, respectively. The present simulation results are similar to those in the previous work [21].

3.6. Effect of domain size

We study the effect of domain size on the formation of lamellar patterns. We first consider the wave-shaped complex region defined in the domain $\Omega = (0, 4\pi) \times (0, 2\pi)$. The initial condition is defined as

$$\phi(x, y, 0) = \begin{cases} 0.001\text{rand}(x, y) & \text{if } f(x) < y < g(x), \\ -0.75 & \text{otherwise,} \end{cases} \quad (15)$$

where $f(x) = -\cos(0.5x) - 1 + (2 - A)\pi$ and $g(x) = \cos(0.5x) + 1 + A\pi$. Here, we use $h = \pi/200$, $\epsilon = 0.0354$, $\Delta t = 0.04h^2$, and $\alpha = 100$. The simulation

is performed in the interior of the complex region and $\phi = -0.75$ is fixed in the rest region as the Dirichlet boundary condition. We vary the size of complex region by changing the value of $A = 0.2, 0.6,$ and 1 . The snapshots of the computational results with respect to different complex regions are illustrated in Fig. 7. It can be observed that the defect is controlled by the size of the complex region.

Next, we consider the formation of lamellar pattern in the elliptic region. The computational domain is $\Omega = (0, 20) \times (0, 20)$. The initial condition is

$$\phi(x, y, 0) = \begin{cases} 0.001\text{rand}(x, y) & \text{if } \sqrt{(x-10)^2/a^2 + (y-10)^2/b^2} < 1, \\ -0.75 & \text{otherwise.} \end{cases} \quad (16)$$

We use $h = 0.04$, $\epsilon = 0.0354$, $\Delta t = 2.5e-5$, and $\alpha = 100$. Here, $a = 4.5$ is fixed and we change the shape of ellipse by changing the value of $b = 4.5, 6.5,$ and 9.8 . We plot the snapshots of the computational results with respect to different domain sizes in Fig. 8. As we can see, the defect shape resembles the shape of the domain boundaries.

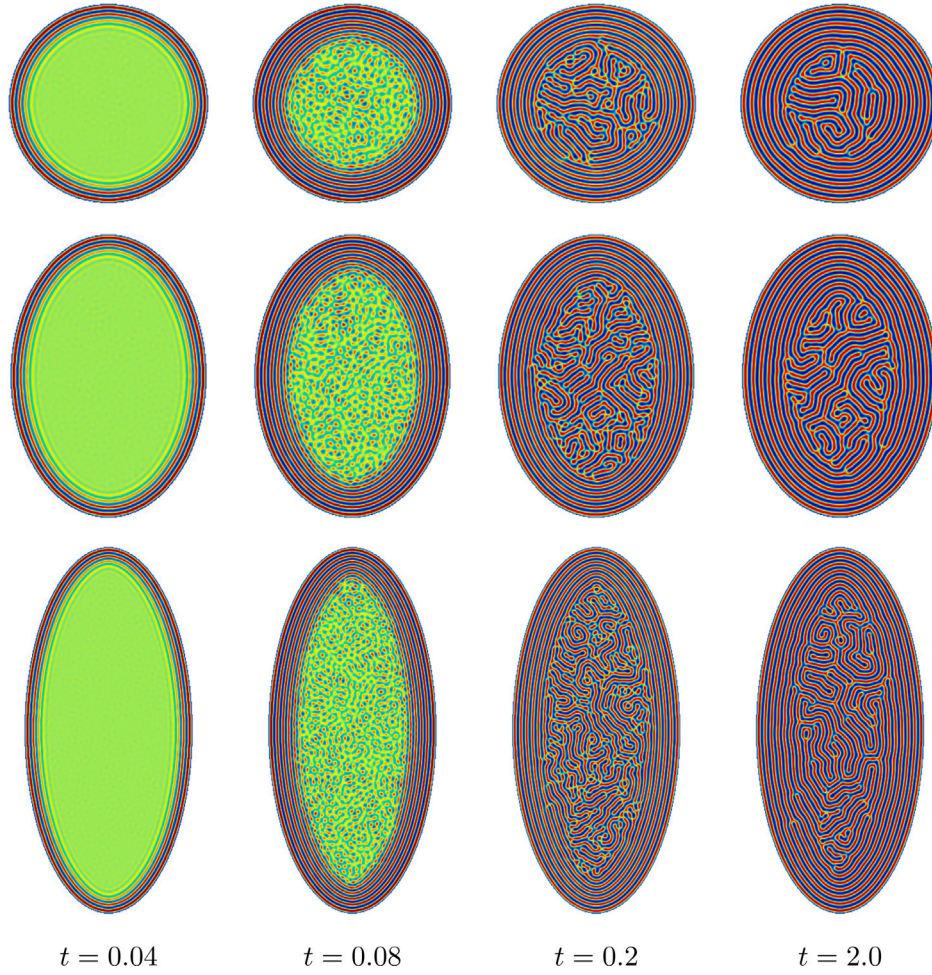


Fig. 8. Pattern formation in the elliptic domains. From top to bottom, $b = 4.5, 6.5,$ and 9.8 .

3.7. Comparison with an implicit type method

For the CH type phase-field models, the nonlinear convex splitting method (CS) is practical because it allows relatively large time steps in the simulations. Some typical works of the CS method for the CH and diblock copolymer equations can refer to [16,22,23]. However, the CS method generally needs extra computational time because the iterative calculations should be performed for the implicit nonlinear term. The fully discrete and temporally first-order accurate scheme for the phase-field diblock copolymer based on the CS method can be written as:

$$\frac{\phi_{ij}^{n+1} - \phi_{ij}^n}{\Delta t} = \Delta_d [(\phi_{ij}^{n+1})^3 - \phi_{ij}^n] - \epsilon^2 \Delta_d^2 \phi_{ij}^{n+1} - \alpha(\phi_{ij}^{n+1} - \bar{\phi}). \quad (17)$$

In this subsection, we verify the efficiency of the proposed method by comparing with the nonlinear CS method. The domain is $\Omega = (0, 150) \times (0, 150)$. The initial state is set to be $\phi(x, y, 0) = -0.3 + 0.15\text{rand}(x, y)$. The parameters are $\Delta t = 0.1h^2$, $h = 1/75$, $\epsilon = 0.01$, and $\alpha = 1000$. Figs. 9(a) and (b) display the snapshots at $t = 0.1422$ with respect to the nonlinear CS method and the proposed Saul'yev method. We find that the results are very consistent. In Fig. 9(c), the CPU time consumed by two different methods is plotted. It can be observed that the proposed method significantly saves computational time. The results plotted in Fig. 9(d) indicate that the energy curves computed by two methods are in good agreement.

3.8. Pattern formations in a complex domain

Now, we consider the pattern formations in a complex domain with spiral shape. The full domain is $\Omega = (-1.6, 1.6) \times (-1.6, 1.6)$. The

schematic illustrations of the formation of a spiral region are shown in Fig. 10. The marker function c is used so that $c = 1$ and $c = 0$ represent the interior and exterior of the complex region, respectively. The simulation is performed in the interior of spiral region and $\phi = -0.75$ is fixed in the rest region as Dirichlet boundary condition. The parameters $h = 3.2/600$, $\epsilon = 0.008$, $\alpha = 1000$, and $\Delta t = 2h^2$ are used. The evolutions with $\bar{\phi} = 0$ and $\bar{\phi} = -0.3$ are shown in the top and bottom rows of Fig. 11. It can be seen that the lamellar and hex-cylinder patterns appear in the complex regions.

4. Discussion

In the present work, we only focus on constructing an efficient Saul'yev method for the phase-field diblock copolymer model and investigating its performance. It should be noted that a temporally second-order accurate scheme is more desirable to perform long-time simulations. In future work, we will extend the current method to a possible second-order time-accurate scheme by using the Crank-Nicolson/Adams-Bashforth (CNAB) approximation as follows.

$$\begin{aligned} & \frac{\phi_{ij}^{n+1} - \phi_{ij}^n}{\Delta t} \\ &= \Delta_d \left[\frac{3}{2} ((\phi_{ij}^n)^3 - \phi_{ij}^n) - \frac{1}{2} ((\phi_{ij}^{n-1})^3 - \phi_{ij}^{n-1}) - \frac{\epsilon^2}{2} (\Delta_d \phi_{ij}^{n+1} + \Delta_d \phi_{ij}^n) \right] \\ & - \alpha \left(\frac{\phi_{ij}^{n+1} + \phi_{ij}^n}{2} - \bar{\phi} \right). \end{aligned} \quad (18)$$

Then, we have one case of eight cases of nested loops:

$$\text{For } j = 1, 2, \dots, N_y, \text{ for } i = 1, 2, \dots, N_x, \quad (19)$$

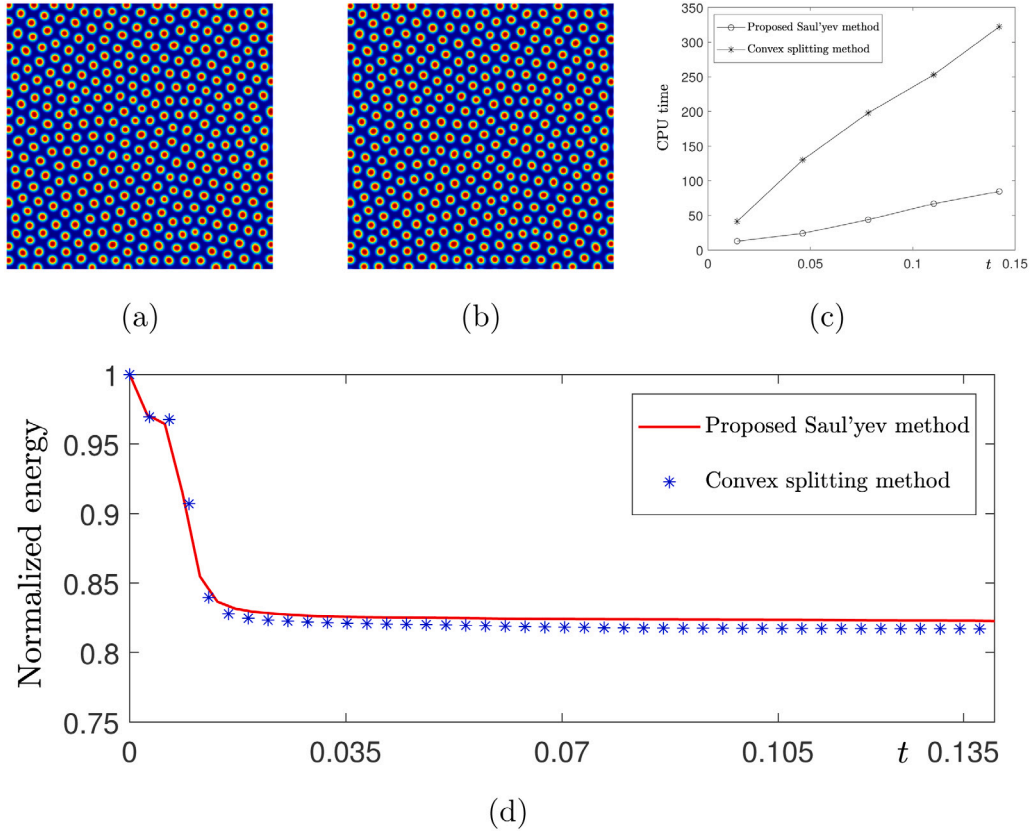


Fig. 9. Patterns computed by (a) the nonlinear CS method and (b) the proposed Saul'yev method. The CPU costs and energy curves are shown in (c) and (d), respectively..

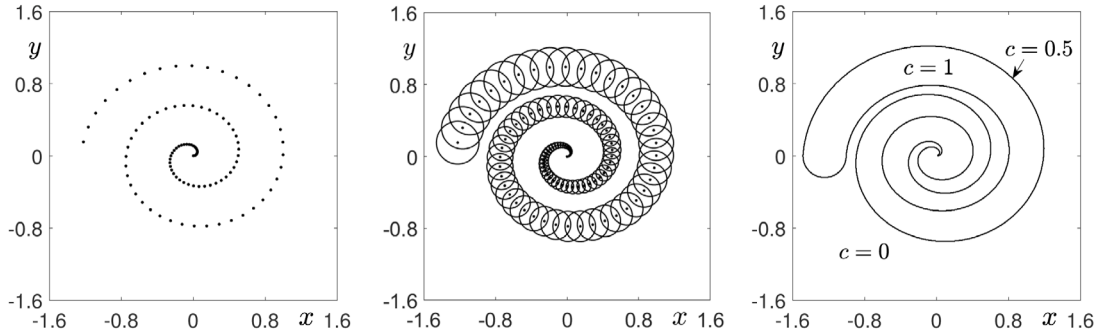


Fig. 10. Schematic illustrations of the formation of complex region.

$$\begin{aligned} \phi_{ij}^{n+1} = & \frac{1}{r} \left\{ \frac{\phi_{ij}^n}{\Delta t} + \Delta_d \left[\frac{3}{2} ((\phi_{ij}^n)^3 - \phi_{ij}^n) - \frac{1}{2} ((\phi_{ij}^{n-1})^3 - \phi_{ij}^{n-1}) + \frac{\epsilon^2}{2} \Delta_d \phi_{ij}^n \right] \right. \\ & + \frac{\epsilon^2}{2h^4} \left[\phi_{i+2,j}^n + \phi_{i-2,j}^{n+1} + \phi_{i,j+2}^n + \phi_{i,j-2}^{n+1} + 2(\phi_{i+1,j+1}^n + \phi_{i+1,j-1}^n \right. \\ & + \phi_{i-1,j+1}^n + \phi_{i-1,j-1}^{n+1}) - 8(\phi_{i+1,j}^n + \phi_{i-1,j}^{n+1} + \phi_{i,j+1}^n + \phi_{i,j-1}^{n+1}) + 10\phi_{ij}^n \left. \right] \\ & \left. - \alpha \left(\frac{\phi_{ij}^n}{2} - \bar{\phi} \right) \right\}, \end{aligned}$$

where $r = 1/\Delta t + 5\epsilon^2/h^4 + \alpha/2$. To update the solution, the above two-step scheme needs the information at $t = n\Delta t$ and $t = (n-1)\Delta t$. In the first time step, we compute (ϕ^1) by using the first-order time-accurate scheme with a subcycling technique. For example, we take four time step iterations with a smaller time $\Delta t/4$ to obtain the numerical solution at $t = \Delta t$ from the given initial condition.

5. Conclusions

In this work, we developed a simple and explicit FDM for the nonlocal CH equation for diblock copolymer melts. The Saul'yev-type scheme was used for the discretizations. Therefore, we can use relatively large time steps. Furthermore, because the proposed method is explicit and it does not require any iterative procedures, the numerical scheme is simple and computationally efficient. The computational results confirmed the superior performance of the proposed method for the phase separation of diblock copolymer melts. In particular, the proposed scheme worked well on complex domains. As upcoming studies, the proposed explicit method will be applied to the diblock copolymer with fluid flows [24].

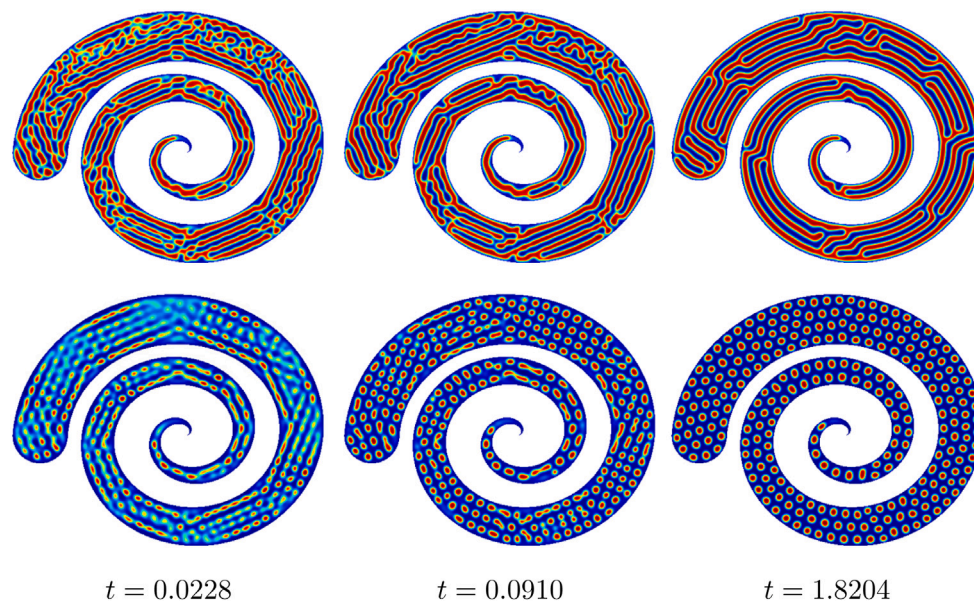


Fig. 11. Pattern formations in complex domain. The top and bottom rows are the results with $\bar{\phi} = 0$ and -0.3 , respectively.

CRedit authorship contribution statement

Junxiang Yang: Conceptualization, Software, Validation, Formal analysis, Investigation, Writing – original draft, Writing – review & editing, Visualization. **Chaeyoung Lee:** Software, Validation, Investigation, Writing – original draft, Writing – review & editing, Visualization, Funding acquisition. **Darae Jeong:** Formal analysis, Investigation, Writing – original draft. **Junseok Kim:** Conceptualization, Methodology, Software, Validation, Formal analysis, Investigation, Writing – original draft, Writing – review & editing, Supervision, Project administration, Funding acquisition.

Declaration of competing interest

The authors declare that they have no known competing financial interests or personal relationships that could have appeared to influence the work reported in this paper.

Data availability

The raw data will be available based on the request to the corresponding author.

Acknowledgments

C. Lee was supported by the National Research Foundation (NRF), Korea, under project BK21 FOUR. The corresponding author (J.S. Kim) was supported by Korea University Grant. The authors appreciate the reviewers for their insightful comments on the revision of this manuscript.

References

- [1] F. Regazzoni, N. Parolini, M. Verani, Topology optimization of multiple anisotropic materials, with application to self-assembling diblock copolymers, *Comput. Methods Appl. Mech. Engrg.* 338 (2018) 562–596.
- [2] P.C. Millett, Mesoscopic simulations of coarsening kinetics within block-copolymer/homopolymer thin films, *Comput. Mater. Sci.* 125 (2016) 20–27.
- [3] X. Xu, Y. Zhao, Energy stable semi-implicit schemes for Allen–Cahn–Ohta–Kawasaki model in binary system, *J. Sci. Comput.* 80 (3) (2019) 1656–1680.
- [4] C. Chen, J. Zhang, X. Yang, Efficient numerical scheme for a new hydrodynamically-coupled conserved Allen–Cahn type Ohta–Kawasaki phase-field model for diblock copolymer melt, *Comput. Phys. Comm.* 256 (2020) 107418.
- [5] J. Zhang, C. Chen, X. Yang, K. Pan, Efficient numerical scheme for a penalized Allen–Cahn type Ohta–Kawasaki phase-field model for diblock copolymers, *J. Comput. Appl. Math.* 378 (2020) 112905.
- [6] X. Xu, Y. Zhao, Maximum principle preserving schemes for binary systems with long-range interactions, *J. Sci. Comput.* 84 (2) (2020) 33, 1–34.
- [7] J. Zhang, C. Chen, X. Yang, Efficient and energy stable method for the Cahn–Hilliard phase-field model for diblock copolymers, *Appl. Numer. Math.* 151 (2020) 263–281.
- [8] J. Zhang, X. Yang, A new magnetic-coupled Cahn–Hilliard phase-field model for diblock copolymers and its numerical approximations, *Appl. Math. Lett.* 107 (2020) 106412.
- [9] Q. Li, L. Mei, Efficient, decoupled, and second-order unconditionally energy stable numerical schemes for the coupled Cahn–Hilliard system in copolymer/homopolymer mixtures, *Comput. Phys. Comm.* 260 (2021) 107290.
- [10] Y. Li, L. Zhang, Q. Xia, Q. Yu, J. Kim, An unconditionally energy-stable second-order time-accurate numerical scheme for the coupled Cahn–Hilliard system in copolymer/homopolymer mixtures, *Comput. Mater. Sci.* 200 (2021) 110809.
- [11] A. Tenneti, D.M. Ackerman, B. Ganapathysubramanian, Equilibrium microstructures of diblock copolymers under 3D confinement, *Comput. Mater. Sci.* 174 (2020) 109453.
- [12] D. Jeong, J. Shin, Y. Li, Y. Choi, J.H. Jung, S. Lee, J. Kim, Numerical analysis of energy-minimizing wavelengths of equilibrium states for diblock copolymers, *Curr. Appl. Phys.* 14 (9) (2014) 1263–1272.
- [13] D. Jeong, J. Kim, Microphase separation patterns in diblock copolymers on curved surfaces using a nonlocal Cahn–Hilliard equation, *Eur. Phys. J. E* 38 (11) (2015) 117.
- [14] Y. Li, Q. Xia, C. Lee, S. Kim, J. Kim, A robust and efficient fingerprint image restoration method based on a phase-field model, *Pattern Recognit.* 123 (2022) 108405.
- [15] S. Yoon, D. Jeong, C. Lee, H. Kim, S. Kim, H.G. Lee, J. Kim, Fourier-spectral method for the phase-field equations, *Mathematics* 8 (8) (2020) 1385.
- [16] J. Shin, J. Kim, An unconditionally gradient stable numerical method for the Ohta–Kawasaki model, *Bull. Korea Math. Soc.* 54 (2017) 145–158.
- [17] J. Shin, H.G. Lee, J.Y. Lee, Convex splitting Runge–Kutta methods for phase-field models, *Comput. Math. Appl.* 73 (11) (2017) 2388–2403.
- [18] M. Dehghan, Saul’yev’s techniques for solving a parabolic equation with a non linear boundary specification, *Int. J. Comput. Math.* 80 (2) (2003) 257–265.
- [19] J. Yang, Y. Li, C. Lee, H.G. Lee, S. Kwak, Y. Hwang, X. Xin, J. Kim, An explicit conservative Saul’yev scheme for the Cahn–Hilliard equation, *Int. J. Mech. Sci.* (2021) in press.
- [20] J. Yang, J. Kim, An energy stable second-order accurate scheme for microphase separation of periodic diblock copolymers, *East Asian J. Appl. Math.* 11 (2) (2021) 234–254.

- [21] D. Jeong, Y. Choi, J. Kim, Numerical investigation of local defectivity control of diblock copolymer patterns, *Condens. Matter Phys.* 19 (3) (2016) 33001, 1–10.
- [22] Y. Yan, W. Chen, C. Wang, S.M. Wise, A second-order energy stable BDF numerical scheme for the Cahn–Hilliard equation, *Commun. Comput. Phys.* 23 (2) (2018) 572–602.
- [23] K. Cheng, W. Feng, C. Wang, S.M. Wise, An energy stable fourth order finite difference scheme for the Cahn–Hilliard equation, *J. Comput. Appl. Math.* 362 (2019) 574–595.
- [24] T. Honda, T. Kawakatsu, Hydrodynamic effects on the disorder-to-order transitions of diblock copolymer melts, *J. Chem. Phys.* 129 (2008) 114904.